Volume 3
Number 4
April 2024
Pages 505–612

Environmental Science Advances

rsc.li/esadvances

ISSN 2754-7000

ROYAL SOCIETY OF CHEMISTRY

PAPER

Alaka Samal, Ajaya K. Behera *et al.*

Design of inexpensive, magnetically separable $MnFe_2O_4$/poly meta-amino phenol (PmAP) heterostructure: catalyst for bisphenol A & reactive blue 19 mineralisation

Environmental Science Advances

ROYAL SOCIETY OF CHEMISTRY

PAPER

View Article Online
View Journal | View Issue

Cite this: *Environ. Sci.: Adv.*, 2024, **3**, 561

Design of inexpensive, magnetically separable $MnFe_2O_4$/poly meta-amino phenol (PmAP) heterostructure: catalyst for bisphenol A & reactive blue 19 mineralisation†

Chirasmayee Mohanty, Priyanka P. Mishra, Alaka Samal, * Nigamananda Das and Ajaya K. Behera *

Organic effluents from industries, especially bisphenol A (BPA) and dyes, pose a growing threat to living creatures due to their resistance to biodegradation and carcinogenic nature. This research emphasizes the design and fabrication of an inexpensive and magnetically separable $MnFe_2O_4$/poly meta-aminophenol heterostructure as a catalyst for the mineralization of two persistent pollutants *viz.* BPA and Reactive Blue 19 (RB-19). The structural and magnetic properties of the $MnFe_2O_4$/PmAP heterostructure (MnP-10) revealed its potential as an efficient and magnetically recoverable catalyst highlighting its practical usability and repeated use in wastewater purification. The heterostructure of MnP-10 was confirmed through various techniques by XRD, XPS, SEM, TEM/HRTEM as well as BET surface area and optical property measurements. The stability and recyclability of the MnP-10 catalyst were confirmed through XRD and VSM studies of fresh and reused catalyst. The catalyst showed 100% efficiency for mineralization of BPA and RB-19 within 60 min of visible light illumination. The TOC and GC-MS analyses confirmed the efficient removal of organic contents after the reaction. The cost-effectiveness and stability of the developed catalyst make it an attractive contender for wastewater treatment applications, addressing the growing concerns connected with the removal of stubborn organic contaminants.

Received 20th December 2023
Accepted 26th February 2024

DOI: 10.1039/d3va00394a

rsc.li/esadvances

Environmental significance

Bisphenol A (BPA) is an artificial chemical that is used to manufacture transparent, durable materials of plastics and epoxy resins. BPA can have a negative impact on reproduction, growth, and development, which raises health and environmental concerns for humans, and aquatic and terrestrial creatures. Additionally, like BPA, RB-19 dye has a hazardous environmental effect. The environment is also at risk from these organic contaminants found in very small amounts in wastewater and its byproducts. Thus, it becomes crucial to address mineralization of these organics, because the adsorption process alone is insufficient. The present work contains synthesis of a new poly meta-amino phenol (PmAP)/$MnFe_2O_4$ composite catalyst for removal of hazardous bisphenol A and reactive blue-19 (RB-19) from contaminated water. Under 60 minutes of visible light exposure, this new catalyst could mineralize a substantial quantity of BPA and RB-19 pollutants. The TOC analysis confirms the fragmentation of the bigger carbon structure with the use of this photocatalyst to smaller compounds.

Introduction

In the modern era, rapid industrialization and a growing population have generated an alarming water pollution issue. The water pollutants *viz.* dyes, microplastics, antibiotics, *etc.* are indeed hazardous chemicals that obstruct natural processes or have a detrimental impact on the environment and living things. In particular, the textile industry discharges ~20% of the whole of the wastewater generated during the dying process of textiles.[1] Reactive dyes are widely used in textile industries,[2] owing to their strong covalent bond between the reactive group and fibre. The hazardous chemical composition of reactive groups in these dyes is teratogenic and carcinogenic to both humans and aquatic life.[3,4] Low quantities of reactive dye colour in water are often invisible to human eyes but have obvious, unpleasant, and dangerous health and environmental effects.[5] Furthermore, bisphenol-A [2,2-bis(4-hydroxyphenyl)propane] (BPA) is widely used in the fabrication of pigments, epoxy resins, glues, retardants, besides different polycarbonates synthesis.[6] On average, first-order wastes from polycarbonate generating units comprise up to 100 mg L^{-1} BPA, which could gather in the atmosphere due to unintended discharge.[6] With an LC50 value of 10 mg L^{-1}, BPA is considered to be poisonous

Department of Chemistry, Utkal University, Bhubaneswar, Odisha, 751004, India. E-mail: samal.alaka@gmail.com; ajayabehera@utkaluniversity.ac.in

† Electronic supplementary information (ESI) available. See DOI: https://doi.org/10.1039/d3va00394a

to crustaceans and the environment.[6] For this, many approaches have been used to address the accumulation of undesired organics in the environment, including chemical oxidation, photocatalytic degradation, filtering, and adsorption. Among all, photocatalysis using a reliable, effective, economical, and non-hazardous catalytic material has been considered a simple and evolving technology for the degradation of organic contaminants. Given that it is a "green" technology for the degradation of organic water pollutants, significant efforts have been put into developing a variety of new photocatalysts.[7–9] However, one of the main issues preventing their widespread use in industry is the reutilization of the catalyst because of the separation challenges. Thus, designing a catalyst that can satisfy all the requirements cited above and will be easily separable with little to no effort is crucial for this photocatalysis technology to be efficient enough.

On account of the fascinating physical and chemical characteristics, ferrite-based transition spinel metal oxides (MFe_2O_4, M = Mn, Fe, Co, Ni, Zn, *etc.*) have attracted a lot of attention.[8] The distinctive magnetic feature of ferrite helps in the recovery of the material easily after the catalytic reaction. Magnetic separation is considered to be a successful method for removing photocatalysts from wastewater to figure out the separation and cost issues. Furthermore, the ferrites as a catalyst are thermally and chemically stable.[10] As a result, nanocomposites prepared through magnetic ferrites-based materials generate photocatalytic systems with improved characteristics, thereby limiting the shortcomings of neat materials.[10–12] Among the most significant magnetic materials, spinel manganese ferrite ($MnFe_2O_4$), has outstanding ferromagnetic behavior at ambient temperature and has found extensive usage in a variety of applications, including cancer therapy, magnetic resonance imaging (MRI), lithium-ion batteries/supercapacitors, catalytic activities, sensors, hydrogen production, heavy metal removal, and drug delivery.[13–16] Due to the affordability, ease of manufacture, chemical resistance, abundance of adsorption sites, and remarkable magnetic characteristics, $MnFe_2O_4$ has been the subject of substantial research in the fields of photocatalysis and energy storage. Additionally, due to the presence of two cations in the same crystal structure of $MnFe_2O_4$, different valences increase the active sites and specific surface area of the material extensively. $MnFe_2O_4$ has better chemical stability, ferromagnetic characteristics, and strong visible light absorption ability, and received more attention than other ferrites.[17–21]

Despite the amazing features, only a handful of research articles were published using manganese ferrite-based catalysts for dye degradation presumably due to the high recombination of the charge carriers in the presence of light. Thus, it was conceptualized that combining this material with a conductive polymer which may drastically improve the performance and stability of the material using a catalyst. Using this idea, some researchers have explored polymer-based manganese ferrite composite for different applications. For instance, Joshi *et al.* reported the polyaniline/$Mn_{0.25}Co_{0.75}Fe_2O_4$ nanocomposites structural and optical characteristics for the photocatalytic degradation of crystal violet dye using visible light.[22] Similarly, Zeng *et al.* reported a quick and practical method for manufacturing a magnetically recyclable $MnFe_2O_4$/PANI composite using an in-place oxidative polymerization process, the catalyst exhibited improved photocatalytic activity in dye removal.[23] Peter *et al.* designed a catalyst of biochar from chromoleana odorata and studied the photosorption of indigo and methylene blue dyes by nanoparticles of $MnFe_2O_4$ and $ZnFe_2O_4$.[24] Recently, a researcher has designed PANI/$MnFe_2O_4$, a sensible composite material for improved photocatalytic activity and energy storage.[25]

Like polyaniline (PANI), poly meta-aminophenol (PmAP), a derivative of PANI is a typical conductive polymer that can be used as a sensitizer of semiconductor-based photocatalysts to significantly improve the photoactivity in photocatalysis process because of its narrow band gap (2.0 eV), high absorption coefficients in the visible light range and high mobility of charge carriers.[26] Aminophenols are interesting electrochemical materials due to the fact that unlike aniline, they include an additional phenol group. Therefore the PmAP shows promising electrochemical activities owing to the synergetic behavior of –OH and $–NH_2$ functional groups. PmAP exhibits the outstanding properties of polyaniline since it is a derivative of that substance. Additionally, PmAP can act as an electron donor and hole acceptor when exposed to visible light and thus can support the high charge separation efficiency in the presence of light.

Herein, a simple and efficient method was presented for *in situ* chemical oxidative polymerization-based synthesis of a magnetically recyclable $MnFe_2O_4$/PmAP composite that showed great photomineralisation ability for BPA and RB 19 dye under visible light irradiation. To the best of our knowledge, this is the first-ever report on the use of $MnFe_2O_4$/PmAP as a cost-effective, magnetically separable, highly reactive visible light active photocatalyst.

Results and discussion

With the use of XRD, the crystallinity, phase purity, and confirmation of the formation of the composite are established. The XRD patterns of PmAP, $MnFe_2O_4$, MnP-30, and MnP-10 composite are represented in Fig. 1a. XRD of PmAP comprised of a broad peak centered at 2θ, 20–30° corresponds to (002) plane, which can be attributed to the periodic PmAP polymer chain structure.[27] All diffraction peaks matched well by position and relative intensity with $MnFe_2O_4$ planes with peak positions at 18.1°, 43.3°, and 47.7° indexed to the presence of the (111), (311), and (222) planes, respectively (Fig. 1a) which exhibited cubic structure of $MnFe_2O_4$.[28] The absence of any other phase or impurity peaks demonstrated that a pure phase of the material was formed. These distinctive peaks of $MnFe_2O_4$ were seen in the $MnFe_2O_4$-PmAP (MnP-10) composite; however, the intensity and position differ slightly. This may be due to the development of a heterojunction interface between two components.[29] Whereas in the case of MnP-30, the diffraction peaks indicate less crystallinity and the positions of the peaks are also shifted; this confirms the non-perfect formation of composite with a higher quantity of PmAP. From this, it can be assumed that

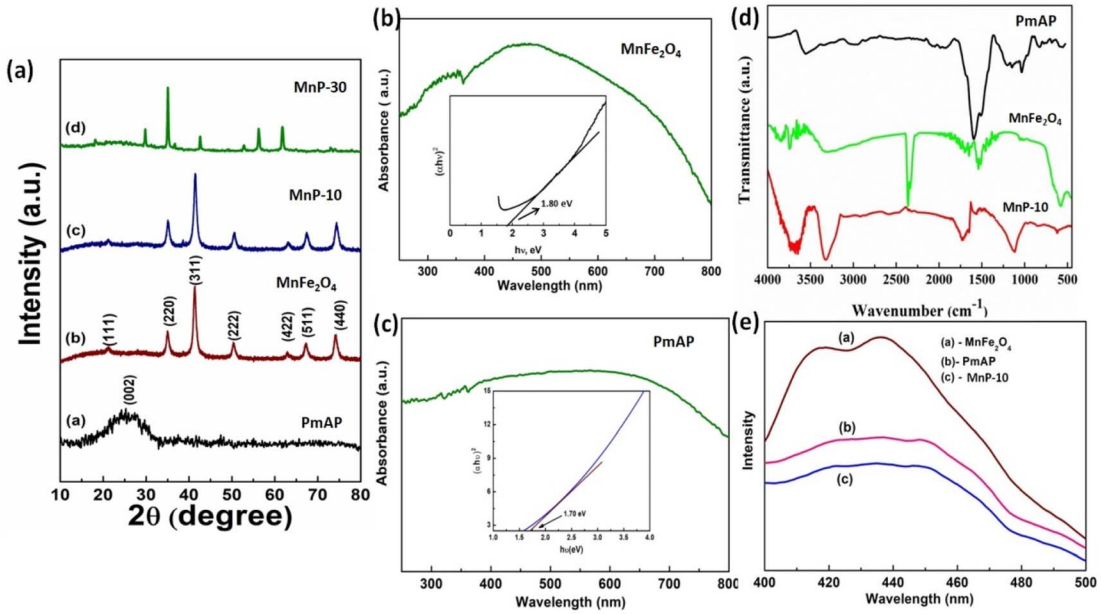

Fig. 1 (a) XRD pattern of $MnFe_2O_4$, PmAP, MnP-10 and 30. (b and c) UV-DRS analysis of $MnFe_2O_4$ and PmAP; (inset) respective band gap energy plot calculated through Kebelka–Monk method. (d) FTIR and (e) PL spectra analysis of $MnFe_2O_4$, PmAP, MnP-10.

MnP-10 will show better results in terms of efficacy and other analytical behavior.

The UV-vis spectra of $MnFe_2O_4$ and PmAP were taken to get an idea about their band gap values and the light absorption efficacy of the composite. Fig. 1b and c displays the UV-visible absorbance spectra of the $MnFe_2O_4$ and PmAP samples along with band gap values calculated from the Tauc's plots. The absorbance spectra revealed that both $MnFe_2O_4$ and PmAP strongly absorb light in the entire visible region with an absorption edge value of 710 nm. The band gap value was calculated from the very well-known Kubelka–Monk method and found to be ~1.8 and 1.7 eV for $MnFe_2O_4$ and PmAP, respectively, and efficient enough to trap the visible light of the sun. Fig. 1d displays the FTIR spectra of PmAP, $MnFe_2O_4$, MnP-10 composite. The peak at 3427 cm^{-1} is ascribed to the NH stretching mode for pure PmAP, whereas the peaks at 1456 and 1577 cm^{-1} are related to the C=C stretching of the benzenoid and quinoid ring structures. Pure $MnFe_2O_4$ has a significant peak at 564 cm^{-1} which refers to Fe–O stretching vibration of ferrite. Similar characteristic bands of PmAP and $MnFe_2O_4$ are also observed in the MnP-10 composite with slight shifting in the peak positions. This further confirms the formation of the heterostructure between the two individual components. To know the charge carrier recombination characteristic, the pure samples and the composite were analyzed through PL spectroscopy as depicted in Fig. 1e. As illustrated from the figure, the MnP-10 composite has the lowest PL intensity in comparison to the bare PmAP, $MnFe_2O_4$. Thus, the PL spectra confirm the lowest recombination of charge carriers upon illumination of light which might be due to the transfer and separation of the e^-/h^+ owing to the formation of heterostructure between PmAP and $MnFe_2O_4$.

The SEM images of the as-synthesized $MnFe_2O_4$, PmAP and MnP-10 composite are shown in Fig. 2. As depicted in the figure, the morphology of $MnFe_2O_4$ discloses tiny flakes sort of particles with 8–9 nm of dimension. The aggregation of nanoparticles might be due to the van der Waals attraction or dipolar interactions between the particles. The PmAP morphology was observed to be a thin flakes-like structure (Fig. 2b). However, the morphology of MnP-10 composite is the combination of $MnFe_2O_4$ particles and the slight amorphous character of the polymer (Fig. 2c). The morphological and EDAX analysis, both the structural feature along its composition of material, confirm the successful synthesis of the heterostructure (Fig. 2d). The EDAX pattern shows that all the components, Fe, Mn, and O, were present and have a precise composition.[30–32]

From the TEM/HRTEM observation of the MnP-10 catalyst, it is worth noting that the $MnFe_2O_4$ nanoparticles are efficiently attached to the polymer sheet. Fig. 3a further shows that the particle size of $MnFe_2O_4$ in MnP-10 composite is small (9–10 nm). Additionally, the MnP-10 SAED pattern (Fig. 3b) also substantiates the formation of $MnFe_2O_4$ on the surface of the PmAP quite effectively. On the one hand, the strong interaction between $MnFe_2O_4$ and PmAP can be seen from the corresponding HRTEM images. Fig. 3c and d shows the HRTEM image with lattice fringes of inter-planar widths of 0.231 nm, which are compatible with the (220) planes of $MnFe_2O_4$.

Additionally, the BET surface areas of neat $MnFe_2O_4$ and MnP-10 were measured to examine the impact of PmAP on the resulting composite and the obtained values are 36.6 and 31.8 $m^2\ g^{-1}$, respectively. A little reduction in specific surface area is seen in the case of MnP-10 composite, which is likely due to the interaction between PmAP and $MnFe_2O_4$ nanocrystals leading to decrease of porosity.

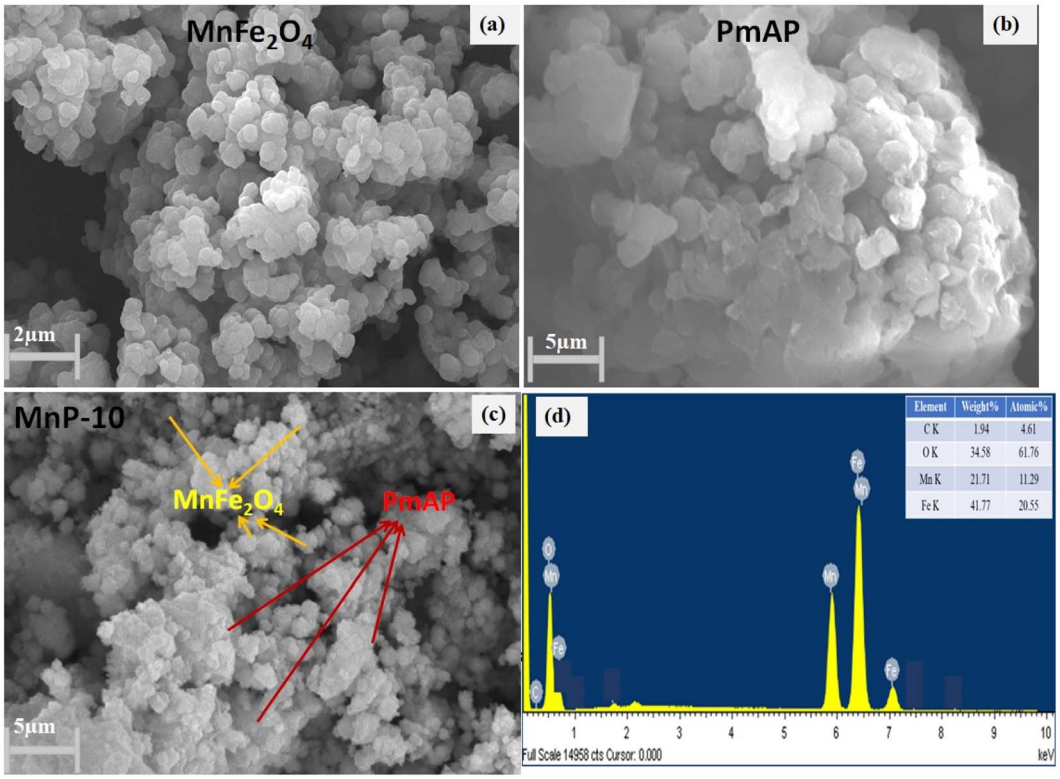

Fig. 2 SEM analysis of (a) $MnFe_2O_4$, (b) PmAP and (c) MnP-10 (d) EDAX spectrum of MnP-10.

The XPS spectrum of MnP-10, $MnFe_2O_4$ and PmAP was presented in Fig. 4 to compare their respective binding energy shifts, and aid in understanding the compositional and electronic structure changes after the formation of the composite. The MnP-10 composite XPS spectra show the composition of all the elements and establish the occurrence of PmAP. The C 1s scan peak of the PmAp and MnP-10 composite clearly indicates the presence of aromatic carbons owing to the polymeric structure of the PmAP (Fig. 4a and d). The N 1s spectrum of PmAp and the composite are displayed in Fig. 4b and e. The deconvoluted line corresponds to C–N, neutral/tertiary amine (C═N), quaternary amine/protonated imine ($C{=}NH^+$), and N–N convey the structural information of PmAP. Whereas the O 1s spectrum (Fig. 4c, f, i and l) corresponds to lattice oxygen, oxides and the surface hydroxyl groups in the pristine and composite samples confirms the presence of oxygen moiety. Mn 2p scan (Fig. 4g and j) represents two peaks, corresponding to the Mn $2p_{3/2}$ and Mn $2p_{1/2}$, respectively. The fitted spectrum of Mn 2p scan represents the material to be in $MnFe_2O_4$ form prominently. The Fe 2p scan (Fig. 4h and k) represents the presence of peaks belonging to binding energies of Fe $2p_{3/2}$ and Fe $2p_{1/2}$, respectively with the shake-up satellite peak, confirming that the main valence of Fe ions is +3 in $MnFe_2O_4$ and MnP-10 composite. This further explains the successful construction of the composite using PmAP and $MnFe_2O_4$. The binding energy shift in the MnP-10 composite was observed might be due to the chemical interactions between constituent elements and thereof distorted electron density.

Mineralization study of BPA & RB-19

The photocatalytic mineralization study of BPA and RB 19 was investigated using the prepared catalysts *viz.* $MnFe_2O_4$, PmAP, and their composites, MnP-10 and MnP-30 under visible light irradiation (Fig. 5). Before being exposed to radiation, the suspension was stirred in the dark for 30 min to attain adsorption–desorption equilibrium. The performance of the samples in dark and light conditions was not significant without the catalyst but in the presence of the catalyst with light illumination, the mineralization gets started immediately. Fig. 5 displays the efficacy of catalysts towards the degradation of organic pollutants with variable concentrations. From these experiments, MnP-10 was found to be the best one (Fig. 5a–c) that could able to mineralize BPA and RB-19 (50 mg L^{-1}) in 60 min of light illumination (Fig. 5d and e). The experimental degradation data were well-fitted to the pseudo-first-order kinetic model (eqn (1)) with high correlation coefficient (R^2) values.

$$\ln(q_e - q_t) = \ln q_e - k_1 t \quad (1)$$

where $\ln(q_e - q_t)$ is plotted against time (t). Here, q_e (mg g^{-1}) and q_t (mg g^{-1}) denote the amounts of dyes/BPA degraded at equilibrium and at time t, respectively, while k_1 (min^{-1}) represents the rate constant of the pseudo-first-order reaction.

To analyze the degradation products after the reaction, TOC analysis was carried out for BPA and RB-19, and its findings are shown in Fig. 6a and b. As seen from the bar graph, the TOC

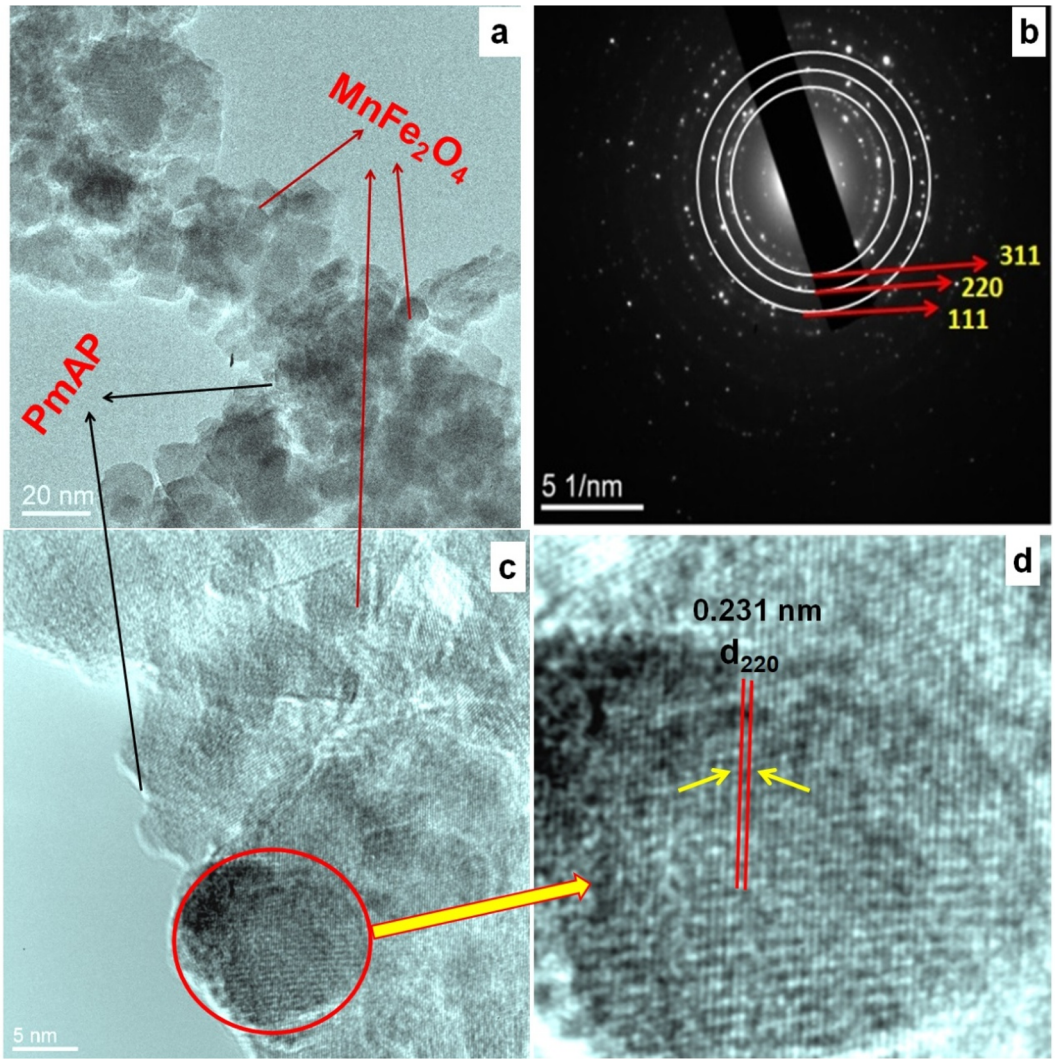

Fig. 3 (a) TEM, (b) SEAD pattern and (c and d) HRTEM analysis of MnP-10 heterostructured system.

decreased noticeably from 83.3 to 13.5% and 87.3 to 16.2% after 0 and 60 min of light exposure for BPA and RB-19, respectively. This validates the mineralization procedure of organics and evidences the fragmentation of the organic molecules to small carbon-based molecules as mineralized products after the photoreaction. To examine the formation of $^{\bullet}OH$ radicals on the surface of the catalyst during the photoreaction, terephthalic acid fluorescent probe experiment was conducted using PL spectroscopy. Fig. 6c represents the peak of 2-hydroxy terephthalic acid, an extremely luminous compound that is formed with the reaction of $^{\bullet}OH$ and terephthalic acid and displays PL emission spectra at 426 nm. From the analysis, it was evident that maximum $^{\bullet}OH$ radicals are being generated on MnP-10 composite that has the highest spectral intensity as compared to the pristine catalysts.

Furthermore, to detect the more active species among $^{\bullet}O_2^-$, e^-, h^+ and $^{\bullet}OH$ involved in the mineralization, the photocatalytic reaction was repeated in the presence of varying scavengers. The active species presence can be seen in Fig. 6d. From the experiments, it was found that both $^{\bullet}O_2^-$ and $^{\bullet}OH$ radicals are responsible for the mineralization of organic molecules.[26] These oxidizing species break down the bulk organic moiety into smaller molecules such as CO_2, H_2O, NO_3^-, NH_4^+, *etc.*[33–35] The intermediate products, generated following the photocatalytic decomposition of BPA and RB-19, were determined using GC-MS as illustrated in Fig. S1 and S2.† According to the intermediates discovered during the GC-MS analysis, the figures described the predicted potential reaction pathways for the degradation of organics. It can be said that the BPA degradation is followed by the formation of hydroquinone, and this aromatic intermediate undergoes a subsequent oxidation process into nontoxic aliphatic acids *via* ring-opening reactions. Finally, these aliphatic acids were oxidized into carbon dioxide and water. In the case of RB-19 degradation, intermediates were recognized as derivatives of anthracene and benzoic acids followed by phthalic acid to form carbon dioxide as the end product. The particular pathway for Reactive Blue 19 degradation is illustrated in Fig. S2.† From the GC-MS and TOC analysis, the mineralization of BPA and RB 19 was confirmed and established. Additionally, this catalyst has excellent reusability

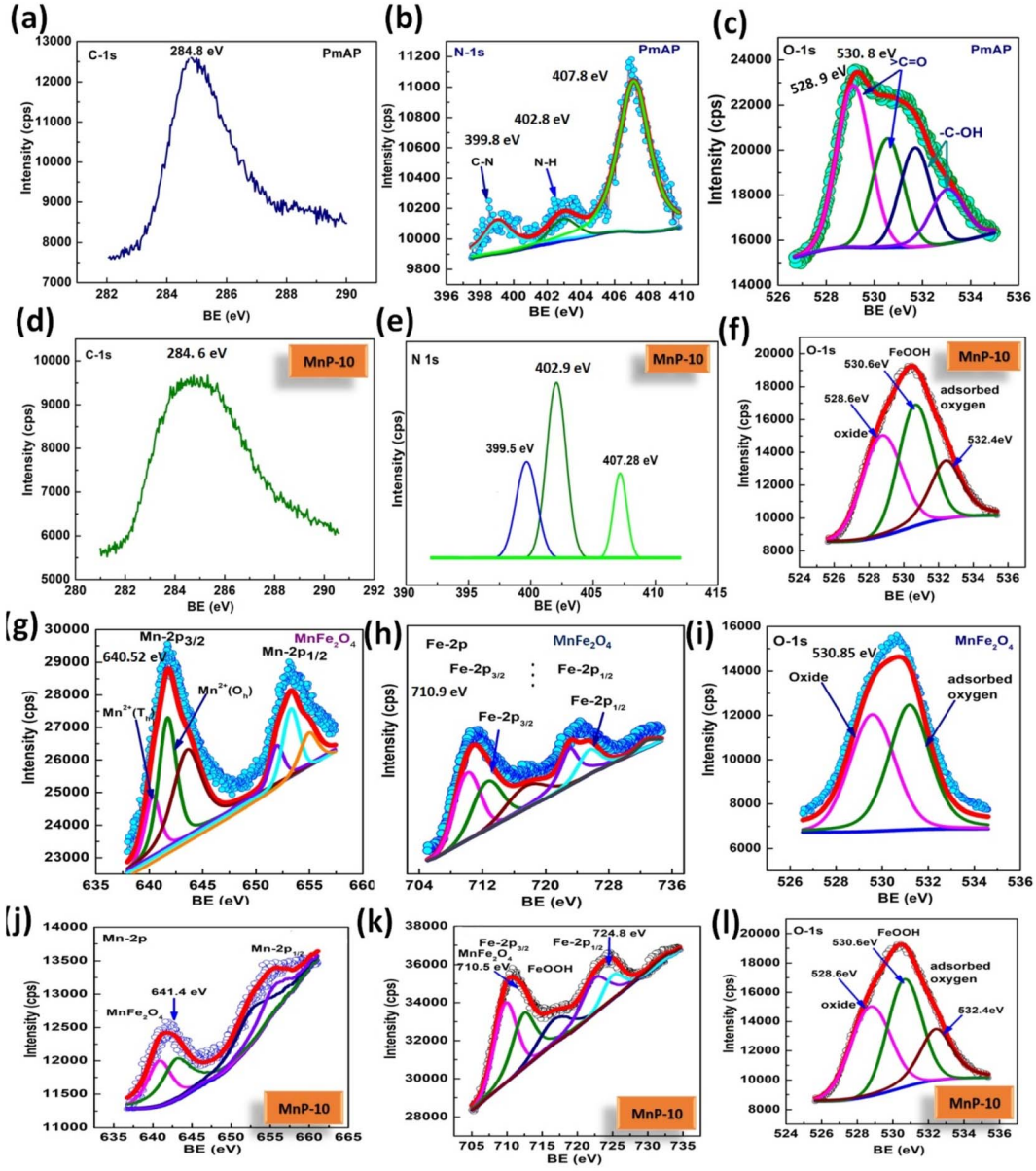

Fig. 4 C 1s, N 1s and O 1s XPS scan of PmAP (a–c) and MnP-10 (d–f). Mn 2p, Fe 2p and O 1s scan of $MnFe_2O_4$ (g–i) and MnP-10 composite (j–l).

as can be seen from Fig. 6e and f including a simple magnetic separation method.

VSM investigations were performed on the materials to verify any alteration in magnetic behavior before and after the reaction. Fig. 7a shows a comparison between the magnetic analysis of the fresh and reused MnP-10 material. The fresh MnP-10 has magnetic saturation values of 39.6 emu g^{-1} after the reaction. A slight diminution in the magnetism of the used catalyst was observed. But still, the catalyst shows strong magnetic behavior, with a saturation magnetization value of almost 35.8 emu g^{-1}. This study conveys that recycling MnP-10 is considerably simpler because of its magnetic properties. To undertake recycling tests, the material can be separated from the reaction mixture using an external magnetic field. Furthermore, Fig. 7b presents XRD assessments of catalysts, before and after reaction. The patterns obtained from XRD show no discernible changes, indicating good stability of the MnP-10 heterostructure. This could provide strong proof that catalysis is stable and effective even over 4th cycle of photoreaction.

Plausible mechanism

The interaction and synergistic effect of both $MnFe_2O_4$ and PmAP are primarily responsible for the considerable improvement of the photocatalytic activity of the MnP-10 catalyst. A schematic illustration of Fig. 8 illustrates the photodegradation process for $MnFe_2O_4$ and PmAP nanocomposite under visible light. The band structure of PmAP was evaluated through the Mott–Schottky analysis (Fig. S3, ESI†). It is considered that the flat band potential of the semiconductor indicates the

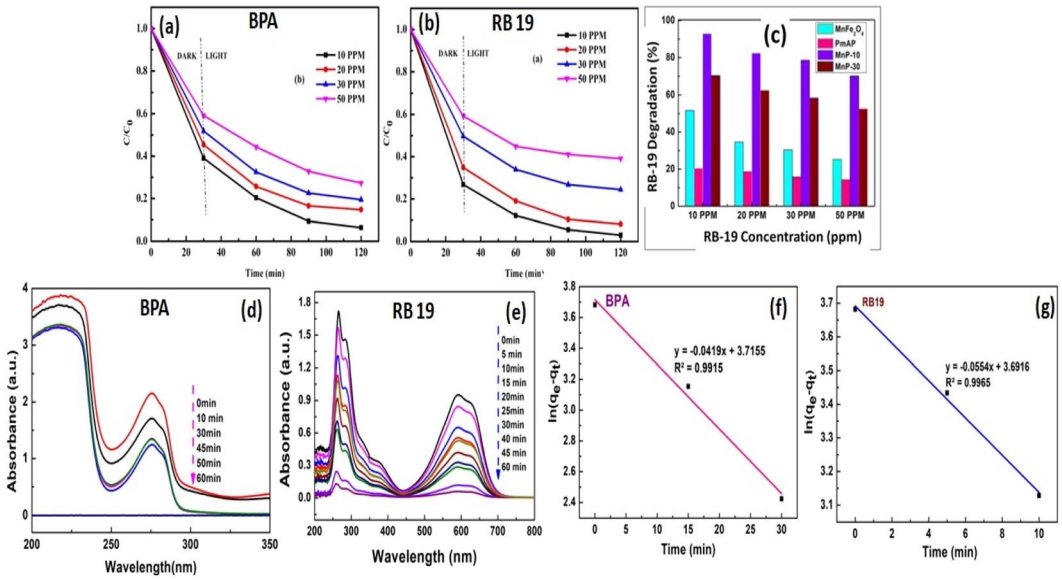

Fig. 5 Effect of illumination time of photodegradation of (a) BPA, (b) RB-19 at different concentrations by MnP-10 (c) comparative photocatalytic analysis of the photodegradation of RB-19 at various concentrations. (d and e) UV-visible absorption spectra of BPA and RB-19 at different times within 0–60 min of the reaction. (f and g) Linear fitting of the visible light degradation profiles to the pseudo-first-order kinetic model of RB 19 and BPA in the presence of MnP-10 catalyst.

approximate location of the conduction band (E_{CB}) for n-type semiconductors and the valence band (E_{VB}) for p-type semiconductors.[36,37] Thus, the E_{VB} and E_{CB} of the PmAp were determined to be +1.33 eV and −0.37 eV, respectively.[36–38] Whereas, $MnFe_2O_4$ ($E_{CB} = -0.61$ eV, $E_{VB} = +1.19$ eV) is a narrow band-gap semiconductor that can absorb visible light and generate pairs of electrons and holes (e^-/h^+).[39] Principally, the following methods might be used to speculate the photocatalytic mechanism for this system as represented in previously reported articles.[40–45] Upon the illumination of visible light on the composite, electrons get excited from the E_{VB} of the semiconductors to their respective E_{CB} creating electron and hole

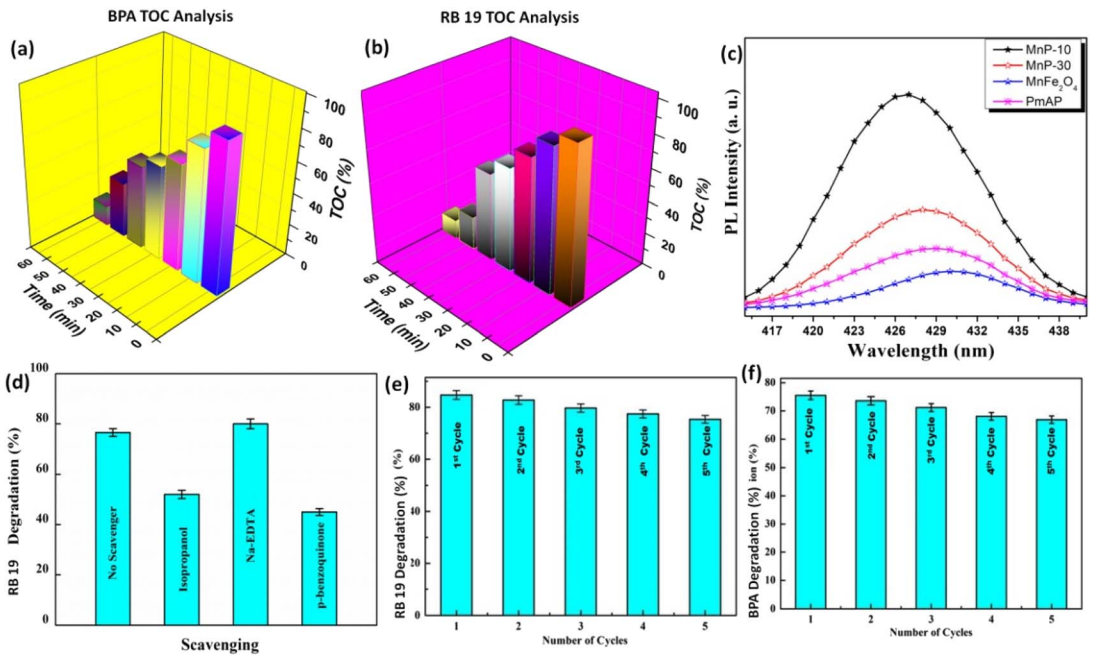

Fig. 6 (a and b) TOC analysis as recorded before and after the photoreaction of BPA and RB-19 (c) fluorescence spectra analysed with 4×10^{-m} NaOH solution of teraphthalic acid (excitation at 315 nm) (d) Scavengers trapping experiments for photodegradation of RB-19 over MnP-10 catalyst. Recyclability of the catalyst MnP-10, for the photodegradation of BPA (e) and RB-19 (f).

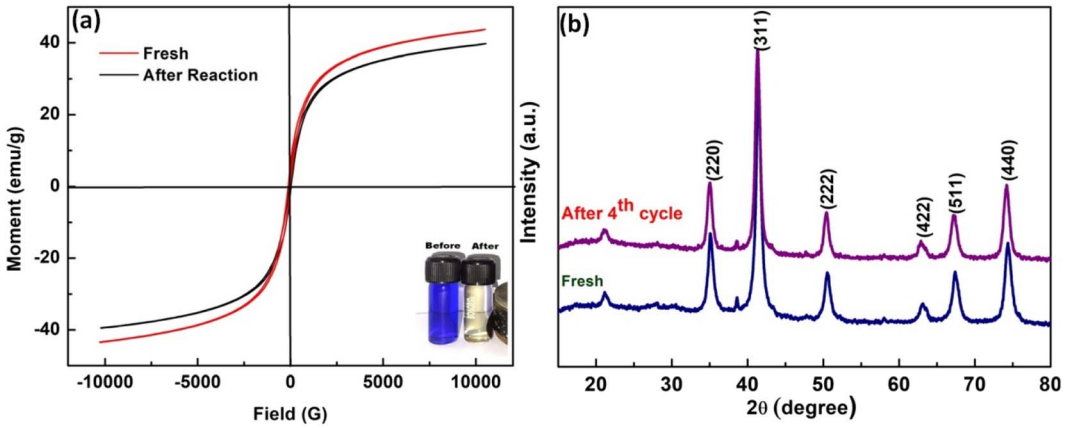

Fig. 7 (a) VSM and (b) XRD result comparison of fresh and reused MnP-10 photocatalyst.

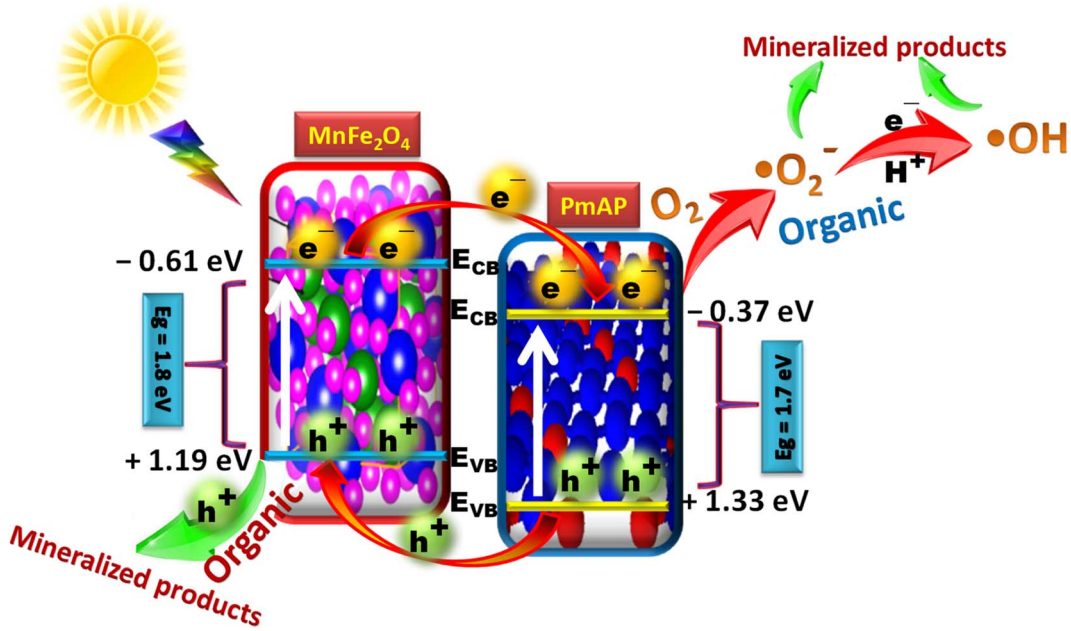

Fig. 8 A plausible mechanism of mineralization of organics using $MnFe_2O_4$-PmAP in the presence of visible light.

pairs. The holes get transferred from E_{VB} of PmAP to E_{VB} of $MnFe_2O_4$ to directly mineralize the organics. It may be noted that both valence bands of semiconductors have insufficient potential to produce $^{\bullet}OH$ radicals (1.99 V *vs.* NHE). But still $^{\bullet}OH$ radical was recognised as a key species from the scavenging and PL studies of MnP-10 catalyst. Hence it is concluded that the electrons get transferred from the conduction band of $MnFe_2O_4$ to the conduction band of PmAP to produce $^{\bullet}O_2^-$ and $^{\bullet}OH$ radicals as per the following reaction steps to help in the mineralization of organics.[45,46]

$$O_2 + e^- \rightarrow {}^{\bullet}O_2^- + H^+ \rightarrow {}^{\bullet}OH_2 + e^- + H^+ \rightarrow H_2O_2 + e^- \rightarrow {}^{\bullet}OH + OH^- \quad (2)$$

Moreover, as per the morphological study of MnP-10 composite, it was observed that the $MnFe_2O_4$ and PmAP interact strongly and create interfaces. Thus, excited state electrons in $MnFe_2O_4$ can easily migrate into PmAP conduction band. Further, due to the coupled electric fields of the two materials, simultaneous holes in the valence band of PmAP migrate to the $MnFe_2O_4$. As a result, photogenerated electrons and holes flow in opposite directions, lowering the possibility of recombination and increasing charge separation efficiency, resulting in increased photocatalytic activity.

Conclusion

In this work, the photocatalytic removal of BPA and RB-19 under visible light was carried out over the simple and non-toxic catalyst, $MnFe_2O_4$/PmAP. A quick and effective approach for creating a magnetically recyclable $MnFe_2O_4$/PmAP composite that has excellent properties and great morphological interaction was established. The recyclability of MnP-10 was examined

for five successive cycles, where it exhibited a very minimal decrease in the percentage of degradation (<3%) after five cycles indicating the stability as well as retaining the activity of the photocatalyst. The organics degradation activity in comparison to other binary and ternary systems with adequate stability of the present composite signifies its potential for practical applications. Photocatalytic removal of these pollutants from actual wastewater using this catalyst needs to be explored to promote real-world applications. In the future, this optimized catalyst combination can be employed for other applications like water splitting, CO_2 reduction, heavy metal removal, *etc.*

Data availability

The data that support the findings of this study are available on request from the corresponding author, AS.

Author contributions

Made substantial contributions to the conception and design of the study and performed data analysis and interpretation: Chirasmayee Mohanty. Performed data acquisition, as well as providing administrative, technical, and material support: Alaka Samal, Ajaya K. Behera, Nigamananda Das. Writing-original draft preparation: Chirasmayee Mohanty, Priyanka Priyadarsini Mishra. Finalization of draft: Alaka Samal, Ajaya K. Behera, Nigamananda Das. All authors have read and agreed to the published version of the manuscript.

Conflicts of interest

All authors declared that there are no conflicts of interest.

Acknowledgements

This research was supported by RUSA 2.0 and DST, Govt. Of Odisha (Project No. 3444/ST). The authors are also grateful to the Department Of Chemistry, Utkal University for providing facilities and support.

References

1 K. Sarayu and S. Sandhya, Current Technologies for Biological Treatment of Textile Wastewater–A Review, *Appl. Biochem. Biotechnol.*, 2012, **167**(3), 645–661.
2 L. Daniela Morais, G. Augusto, G. Meireles, L. Barroso Brito, L. de Rodrigues and D. Palma, Eco- and Genotoxicological Assessments of Two Reactive Textile Dyes, *J. Toxicol. Environ. Health*, 2015, **78**(5), 287–300.
3 E. Sudova, J. Machova, Z. Svobodova and T. Vesely, Negative effects of malachite green and possibilities of its replacement in the treatment of fish eggs and fish: a review, *Vet. Med.*, 2008, **52**(12), 527–539.
4 K. Kabra, R. Chaudhary and R. L. Sawhney, Treatment of Hazardous Organic and Inorganic Compounds through Aqueous-Phase Photocatalysis: A Review, *Ind. Eng. Chem. Res.*, 2004, **43**(24), 7683–7696.
5 M. Kong, Y. Li, X. Chen, T. Tian, P. Fang, F. Zheng, *et al.*, Tuning the Relative Concentration Ratio of Bulk Defects to Surface Defects in TiO_2 Nanocrystals Leads to High Photocatalytic Efficiency, *J. Am. Chem. Soc.*, 2011, **133**(41), 16414–16417.
6 H. Mohan, V. Sethumathavan, S. W. Lee, J. M. Lim, N. Lovanh, Y. J. Park, *et al.*, Improved visible-light-driven photocatalytic removal of Bisphenol A using V_2O_5/WO_3 decorated over Zeolite: Degradation mechanism and toxicity, *Environ. Res.*, 2022, **212**, 113136.
7 H. Yang, C. Zhang, X. Shi, H. Hu, X. Du, Y. Fang, *et al.*, Water-soluble superparamagnetic manganese ferrite nanoparticles for magnetic resonance imaging, *Biomaterials*, 2010, **31**(13), 3667–3673.
8 A. Mittal, J. Mittal, A. Malviya, D. Kaur and V. K. Gupta, Adsorption of hazardous dye crystal violet from wastewater by waste materials, *J. Colloid Interface Sci.*, 2010, **343**(2), 463–473.
9 J. Zhang, Q. Zhou and L. Ou, Kinetic, isotherm, and thermodynamic studies of the adsorption of methyl orange from aqueous solution by chitosan/alumina composite, *J. Chem. Eng. Data*, 2012, **57**(2), 412–419.
10 A. B. Mapossa, W. Mhike, J. L. Adalima and S. Tichapondwa, Removal of organic dyes from water and wastewater using magnetic ferrite-based titanium oxide and zinc oxide nanocomposites: a review, *Catalysts*, 2021, **11**(12), 1543.
11 E. O. Ichipi, A. B. Mapossa, A. C. Costa, E. M. Chirwa and S. M. Tichapondwa, Fabrication and characterization of recyclable, magnetic $(CoFe_2O_4)x/Ag_2S$-ZnO composites for visible-light-induced photocatalytic degradation of methylene blue dye, *J. Water Process Eng.*, 2023, **54**, 104040.
12 P. L. de Oliveira, N. S. Lima, A. C. de Melo Costa, E. B. Cavalcanti and L. de Sousa Conrado, Obtaining TiO2: $CoFe_2O_4$ nanocatalyst by Pechini method for diuron degradation and mineralization, *Ceram. Int.*, 2020, **46**(7), 9421–9435.
13 N. Akhlaghi and G. Najafpour-Darzi, Manganese ferrite $(MnFe_2O_4)$ Nanoparticles: From synthesis to application-A review, *J. Ind. Eng. Chem.*, 2021, **103**, 292–304.
14 K. Asghar, M. Qasim and D. Das, Preparation and characterization of mesoporous magnetic $MnFe_2O_4$@ $mSiO_2$ nanocomposite for drug delivery application, *Mater. Today: Proc.*, 2020, **26**, 87–93.
15 M. M. Cruz, L. P. Ferreira, J. Ramos, S. G. Mendo, A. F. Alves, M. Godinho and M. D. Carvalho, Enhanced magnetic hyperthermia of $CoFe_2O_4$ and $MnFe_2O_4$ nanoparticles, *J. Alloys Compd.*, 2017, **703**, 370–380.
16 F. He, Y. Ji, Y. Wang and Y. Zhang, Preparation of bifunctional hollow mesoporous Fe0@ C@ $MnFe_2O_4$ as Fenton-like catalyst for degradation of Tetrabromobisphenol A, *J. Taiwan Inst. Chem. Eng.*, 2017, **80**, 553–562.
17 D. S. Mathew and R. S. Juang, An overview of the structure and magnetism of spinel ferrite nanoparticles and their synthesis in microemulsions, *Chem. Eng. J.*, 2007, **129**(1–3), 51–65.

18 K. K. Kefeni, B. B. Mamba and T. A. Msagati, Application of spinel ferrite nanoparticles in water and wastewater treatment: a review, *Sep. Purif. Technol.*, 2017, **188**, 399–422.
19 D. H. Reddy and Y. S. Yun, Spinel ferrite magnetic adsorbents: alternative future materials for water purification?, *Coord. Chem. Rev.*, 2016, **315**, 90–111.
20 N. Akhlaghi and G. Najafpour-Darzi, Manganese ferrite ($MnFe_2O_4$) Nanoparticles: From synthesis to application-A review, *J. Ind. Eng. Chem.*, 2021, **103**, 292–304.
21 A. Manohar, V. Vijayakanth, S. P. Vattikuti and K. H. Kim, Synthesis and characterization of Mg^{2+} substituted $MnFe_2O_4$ nanoparticles for supercapacitor applications, *Ceram. Int.*, 2022, **48**(20), 30695–30703.
22 C. S. Joshi, R. C. Srivastava and A. Joshi, Polyaniline/Manganese-Cobalt ferrite nanocomposite as an efficient material for crystal violet dye degradation under sunlight irradiation, *Mater. Today: Proc.*, 2023, DOI: **10.1016/j.matpr.2023.04.462**.
23 S. Zeng, J. Yang, X. Qiu, Z. Liang and Y. Zhang, Magnetically recyclable $MnFe_2O_4$/polyaniline composite with enhanced visible light photocatalytic activity for rhodamine B degradation, *J. Ceram. Soc. Jpn.*, 2016, **124**(10), 1152–1156.
24 P. A. Ajibade and E. C. Nnadozie, Synthesis and structural studies of manganese ferrite and zinc ferrite nanocomposites and their use as photoadsorbents for indigo carmine and methylene blue dyes, *ACS Omega*, 2020, **5**(50), 32386–32394.
25 B. P. Prasanna, D. N. Avadhani, M. S. Raghu and Y. Kumar, Synthesis of polyaniline/α-Fe_2O_3 nanocomposite electrode material for supercapacitor applications, *Mater. Today Commun.*, 2017, **12**, 72–78.
26 A. K. Behera, B. Adhikari and P. Kar, Synthesis of processable conducting poly (m-aminophenol) having structure like keto derivative of polyaniline, *Polym. Sci., Ser. B*, 2015, **57**, 159–166.
27 C. Mohanty, N. Das, A. K. Behera and B. C. Tripathy, Efficiency of Poly (m-Aminophenol) as a Novel Adsorbent for Individual/Simultaneous Removal of Organic Dyes and Hexavalent Chromium from Water Sources, *Water, Air, Soil Pollut.*, 2023, **234**(3), 204.
28 R. Rahimi, H. Kerdari and M. Rabbani, Adsorptive removal of crystal violet (CV), a carcinogenic textile dye, from aqueous solution by conducting polyaniline/hollow manganese ferrite nanocomposites, in *Proceedings of the ECSOC-14: the 14th International Electronic Conference on Synthetic Organic Chemistry*, Basel, Switzerland, 2010, pp. 1–30.
29 V. Eskizeybek, F. Sarı, H. Gülce, A. Gülce and A. Avcı, Preparation of the new polyaniline/ZnO nanocomposite and its photocatalytic activity for degradation of methylene blue and malachite green dyes under UV and natural sun lights irradiations, *Appl. Catal., B*, 2012, **119**, 197–206.
30 S. Khalili, B. Khoshandam and M. Jahanshahi, Optimization of production conditions for synthesis of chemically activated carbon produced from pine cone using response surface methodology for CO_2 adsorption, *RSC Adv.*, 2015, **5**(114), 94115–94129.
31 A. Mittal, J. Mittal, A. Malviya, D. Kaur and V. K. Gupta, Adsorption of hazardous dye crystal violet from wastewater by waste materials, *J. Colloid Interface Sci.*, 2010, **343**(2), 463–473.
32 J. Zhang, Q. Zhou and L. Ou, Kinetic, isotherm, and thermodynamic studies of the adsorption of methyl orange from aqueous solution by chitosan/alumina composite, *J. Chem. Eng. Data*, 2012, **57**(2), 412–419.
33 S. K. Ponnaiah, P. Periakaruppan, B. Vellaichamy and B. Nagulan, Efficacious separation of electron–hole pairs in CeO_2-Al_2O_3 nanoparticles embedded GO heterojunction for robust visible-light driven dye degradation, *J. Colloid Interface Sci.*, 2018, **512**, 219–230.
34 H. Lachheb, E. Puzenat, A. Houas, M. Ksibi, E. Elaloui, C. Guillard and J. M. Herrmann, Photocatalytic degradation of various types of dyes (Alizarin S, Crocein Orange G, Methyl Red, Congo Red, Methylene Blue) in water by UV-irradiated titania, *Appl. Catal., B.*, 2002, **39**(1), 75–90.
35 Y. Chen, J. Yang, X. Wang, F. Feng, Y. Zhang and Y. Tang, Synthesis YFeO3 by salt-assisted solution combustion method and its photocatalytic activity, *J. Ceram. Soc. Jpn.*, 2014, **122**(1422), 146–150.
36 A. J. Bard, Design of semiconductor photoelectrochemical systems for solar energy conversion, *J. Phys. Chem.*, 1982, **86**(2), 172–177.
37 A. Samal, D. P. Das and M. Giridhar, Repercussion of Solid state vs. Liquid state synthesized p–n heterojunction RGO-copper phosphate on proton reduction potential in water, *Sci. Rep.*, 2018, **8**(1), 2881.
38 P. K. Sarswat, D. Bhattacharyya, M. L. Free and M. Misra, Augmented Z scheme blueprint for efficient solar water splitting system using quaternary chalcogenide absorber material, *Phys. Chem. Chem. Phys.*, 2016, **18**(5), 3788–3803.
39 X. Wang, L. Jiang, K. Li, J. Wang, D. Fang, Y. Zhang, D. Tian, Z. Zhang and D. D. Dionysiou, Fabrication of novel Z-scheme $SrTiO_3$/$MnFe_2O_4$ system with double-response activity for simultaneous microwave-induced and photocatalytic degradation of tetracycline and mechanism insight, *Chem. Eng. J.*, 2020, **400**, 125981.
40 S. Zeng, J. Yang, X. Qiu, Z. Liang and Y. Zhang, Magnetically recyclable $MnFe_2O_4$/polyaniline composite with enhanced visible light photocatalytic activity for rhodamine B degradation, *J. Ceram. Soc. Jpn.*, 2016, **124**(10), 1152–1156.
41 H. Feng, J. Yu, L. Tang, J. Wang, H. Dong, T. Ni, J. Tang, W. Tang, X. Zhu and C. Liang, Improved hydrogen evolution activity of layered double hydroxide by optimizing the electronic structure, *Appl. Catal., B*, 2021, **297**, 120478.
42 Y. Y. Yang, C. G. Niu, D. W. Huang, H. Guo, H. P. Feng, L. Li, H. Y. Liu, Q. Q. Fan and M. Z. Qin, Appropriate oxygen vacancies and Mo-N bond synergistically modulate charge transfer dynamics of MoO_3− x/S-CN for superior photocatalytic disinfection: Unveiling synergistic effects and disinfection mechanism, *J. Hazard. Mater.*, 2023, **445**, 130481.

43 H. Feng, J. Yu, J. Tang, L. Tang, Y. Liu, Y. Lu, J. Wang, T. Ni, Y. Yang and Y. Yi, Enhanced electro-oxidation performance of FeCoLDH to organic pollutants using hydrophilic structure, *J. Hazard. Mater.*, 2022, **430**, 128464.

44 A. Samal and P. Das, An Effective Strategy for the Photocatalytic Elimination of Industrial Wastewaters Via MgFe-LDH/TiO_2 Heterojunctions, *Int. Multidiscip. Res. J.*, 2024, **6**(1), 1–16.

45 E. Casbeer, V. K. Sharma and X. Z. Li, Synthesis and photocatalytic activity of ferrites under visible light: a review, *Sep. Purif. Technol.*, 2012, **87**, 1–4.

46 A. Samal, D. P. Das, K. K. Nanda, B. K. Mishra, J. Das and A. Dash, Reduced graphene oxide–Ag_3PO_4 heterostructure: a direct Z-scheme photocatalyst for augmented photoreactivity and stability, *Chem.–Asian J.*, 2016, **11**(4), 584–595.